

University of Groningen

## Variable-parameter NiTi ultrasonic spot welding with Cu interlayer

Ao, S. S.; Zhang, W.; Li, C. J.; Oliveira, J. P.; Zeng, Z.; Luo, Z.

*Published in:*  
Materials and Manufacturing Processes

*DOI:*  
[10.1080/10426914.2020.1843676](https://doi.org/10.1080/10426914.2020.1843676)

**IMPORTANT NOTE: You are advised to consult the publisher's version (publisher's PDF) if you wish to cite from it. Please check the document version below.**

*Document Version*  
Publisher's PDF, also known as Version of record

*Publication date:*  
2021

[Link to publication in University of Groningen/UMCG research database](#)

*Citation for published version (APA):*

Ao, S. S., Zhang, W., Li, C. J., Oliveira, J. P., Zeng, Z., & Luo, Z. (2021). Variable-parameter NiTi ultrasonic spot welding with Cu interlayer. *Materials and Manufacturing Processes*, 36(5), 599-607. <https://doi.org/10.1080/10426914.2020.1843676>

### Copyright

Other than for strictly personal use, it is not permitted to download or to forward/distribute the text or part of it without the consent of the author(s) and/or copyright holder(s), unless the work is under an open content license (like Creative Commons).

The publication may also be distributed here under the terms of Article 25fa of the Dutch Copyright Act, indicated by the "Taverne" license. More information can be found on the University of Groningen website: <https://www.rug.nl/library/open-access/self-archiving-pure/taverne-amendment>.

### Take-down policy

If you believe that this document breaches copyright please contact us providing details, and we will remove access to the work immediately and investigate your claim.

*Downloaded from the University of Groningen/UMCG research database (Pure): <http://www.rug.nl/research/portal>. For technical reasons the number of authors shown on this cover page is limited to 10 maximum.*

## Variable-parameter NiTi ultrasonic spot welding with Cu interlayer

S. S. Ao, W. Zhang, C. J. Li, J. P. Oliveira, Z. Zeng & Z. Luo

To cite this article: S. S. Ao, W. Zhang, C. J. Li, J. P. Oliveira, Z. Zeng & Z. Luo (2021) Variable-parameter NiTi ultrasonic spot welding with Cu interlayer, Materials and Manufacturing Processes, 36:5, 599-607, DOI: [10.1080/10426914.2020.1843676](https://doi.org/10.1080/10426914.2020.1843676)

To link to this article: <https://doi.org/10.1080/10426914.2020.1843676>



Published online: 18 Dec 2020.



Submit your article to this journal [↗](#)



Article views: 172




View related articles [↗](#)



View Crossmark data [↗](#)



## Variable-parameter NiTi ultrasonic spot welding with Cu interlayer

S. S. Ao<sup>a</sup>, W. Zhang <sup>a,b</sup>, C. J. Li<sup>a</sup>, J. P. Oliveira<sup>c,d</sup>, Z. Zeng<sup>e</sup>, and Z. Luo<sup>a</sup>

<sup>a</sup>School of Material Science and Engineering, Tianjin University, Tianjin, China; <sup>b</sup>Department of Advanced Production Engineering, Faculty of Science and Engineering, University of Groningen, Groningen, The Netherlands; <sup>c</sup>UNIDEMI, Department of Mechanical and Industrial Engineering, NOVA School of Science and Technology, NOVA University Lisbon, Caparica, Portugal; <sup>d</sup>CENIMAT/I3N, Department of Materials Science, NOVA School of Science and Technology, Universidade NOVA de Lisboa, Caparica, Portugal; <sup>e</sup>School of Mechanical and Electrical Engineering, University of Electronic Science and Technology of China, Sichuan, China

### ABSTRACT

NiTi thin sheets were ultrasonic spot welded with a Cu interlayer, where different welding vibration amplitudes were applied to study the influence on the surface and interface microstructural characteristics, phase transformation behavior and mechanical response of the joints, which aimed to enhance the joint performance by proper optimization of the process parameters. An excellent bonding interface was achieved when an optimized vibration amplitude was applied, with a recrystallized microstructure formed in the Cu foil side near the bonding interface, which helped to improve the mechanical performance of the joints. Joints made with vibration amplitude of 55  $\mu\text{m}$  had an improved strength compared to the NiTi base material.

### ARTICLE HISTORY

Received 28 June 2020  
Accepted 5 October 2020

### KEYWORDS

Ultrasonic; welding; NiTi; interlayer; parameter; microstructure; performance; fracture

### Introduction

NiTi shape memory alloys (SMAs) are known as smart engineering materials which exhibit excellent mechanical resistance, in addition to the shape memory effect and superelasticity.<sup>[1–3]</sup> These properties, combined with their biocompatibility, render NiTi to be highly appreciated in biomedical, aerospace, and civil engineering applications.<sup>[4–6]</sup> Nowadays, to further expand the potential applications of NiTi SMAs, it is necessary to develop joining methods with high efficiency and reliability owing to the difficulty in machining these materials. Different joining techniques such as laser<sup>[7–10]</sup> and electron beam welding<sup>[11]</sup> have been applied to obtain complex welding structures based on NiTi. However, traditional fusion welding methods give rise to the occurrence of potentially brittle intermetallic compounds and significantly influence the phase transformation behavior in the welded region.<sup>[1,7]</sup> These microstructural-induced changes result from the high-temperature thermal cycles during the welding process and have the tendency to limit the application conditions of these joints. To solve the above-mentioned problems, it is necessary to apply a processing method which can successfully achieve sound welding of NiTi, while persevering its functional and mechanical properties.

As a solid-state welding technique, ultrasonic spot welding (USW) has advantages such as short welding cycle, low peak temperatures, high energy efficiency,<sup>[12]</sup> which is applicable for joining multiple dissimilar materials<sup>[13]</sup> and miniature work pieces.<sup>[14,15]</sup> The potential of this technique to avoid the formation of brittle phases in NiTi joints makes USW a worthy case study for these advanced materials.

Previously, it was observed that after USW, a two-step martensitic transformation occurred potentially due to the formation of  $\text{Ni}_4\text{Ti}_3$  in the welded joints.<sup>[16]</sup> Considering the possible formation of precipitates in the weld region, it is suggested that the

addition of an interlayer can control the microstructural evolution of the weld and improve the mechanical properties of joints.<sup>[17]</sup> As a soft metal, Cu exhibits not only excellent thermal and electrical conductivity, but also a good metallurgical compatibility with NiTi SMAs.<sup>[18–20]</sup> As such, Cu interlayer has been applied in laser welding of NiTi SMAs to  $\text{Ti}_6\text{Al}_4\text{V}$  and stainless steel<sup>[21,22]</sup> in order to limit the formation of brittle intermetallic compounds and therefore, enhance the mechanical properties of the joints. In our previous research work,<sup>[23,24]</sup> the insertion of a Cu interlayer during USW of NiTi resulted in an improvement of the mechanical properties due to a better metallurgical adhesion at the weld interface. However, a detailed study on the effects of USW processing parameters on the microstructural characteristics and properties of SMAs does not exist in the literature.

The present work aims to improve the joining quality of USWed NiTi joints through a variable-parametric study and, in parallel, understand the microstructure and properties of the NiTi joints using a Cu interlayer. For this purpose, in this study, effects of vibration amplitude, which was found to be the most influential welding parameter by screening experiments (refer to the supplementary material appended to this paper), on the weld microstructure, phase transformation characterizations, and tensile properties were thoroughly clarified.

### Materials and methods

NiTi sheets with a composition of 50.8 at. % Ni were used throughout this investigation. The sample dimensions are 60 mm×20 mm×0.2 mm. The preexisting oxide layer on the surface of NiTi was removed with a 20%  $\text{HNO}_3$ , 7.5% HF, and 72.5%  $\text{H}_2\text{O}$  (in volume) etching solution before welding. Pure Cu foils of 100  $\mu\text{m}$  thickness were selected as interlayer.

USW process was performed using an ultrasonic metal welder (SONICS MSC4000-20). Varying vibration amplitudes from 45 to 65  $\mu\text{m}$  with increasing steps of 5  $\mu\text{m}$  were selected to study the effects on the microstructure and performance of the USW joints, while the welding energy and clamping pressure were kept at constant values of 1000 J and 0.4 MPa, respectively.

Surface appearance of different welds was observed with a 3D digital microscope. The specimens for metallography were prepared according to conventional metallographic procedures which involved polishing up to a mirror-like surface with diamond paste. Scanning electron microscopy (SEM) was used for fine observation of the interfacial areas on the transverse section center of different NiTi welds to understand the bonding mechanisms at the faying interface. Meanwhile, electron backscatter diffraction (EBSD) was performed on the weld interface to obtain further crystallographic information.

Differential scanning calorimetry (DSC) measurements of the welded joints were conducted using a constant cooling/heating speed of 10°C/min. The test samples were cut across the center of the welding spot region with a total mass of about 10 mg as shown in Fig. 1. The temperature range for the DSC analysis varied between  $-90^{\circ}\text{C}$  and  $100^{\circ}\text{C}$ . The evaluation of the mechanical properties was conducted by tensile lap-shear tests with the load applied perpendicularly to the ultrasonic vibration direction, and a cross-head speed of 0.01 mm/s was set to determine the joint failure load. Figure 1 depicts the dimensions of the samples used for mechanical testing. Three

specimens were tested for each experimental condition. Finally, SEM was used to characterize the fracture morphology.

## Results and discussion

Representative surface appearances of the USWed NiTi joints obtained with different vibration amplitudes are depicted in Fig. 2. Surface appearances show that indentations on both sides (top surface for the side near the sonotrode and bottom surface for the side near the anvil) are distinct. It can be noticed that the plastic deformation on both surfaces became more significant when higher vibration amplitude levels were used.

Upon the USW process, the sonotrode tip exerts shear stress on the base material (BM) surface by vibrational friction. Then, the repeated motion of slippage and friction is generated at the weld interface, which is fundamental for frictional heat and plastic deformation to occur in the weld region.<sup>[25,26]</sup> The plastic deformation on the material surface occurred mainly due to two types of thermo-mechanical solicitation: surface friction dissipation and softening by volume ultrasonic effect.<sup>[27]</sup> These are credited for decreasing the yield strength of the joints, though contributing for the creation of a sound metallurgical bonding along the weld interface. During the USW process, the average temperature around the weld interface is known to increase as the vibration amplitude increases,<sup>[28]</sup> suggesting the occurrence of significant heat generation due to higher frictional vibration levels. Therefore, the surface friction energy dissipation became faster after the

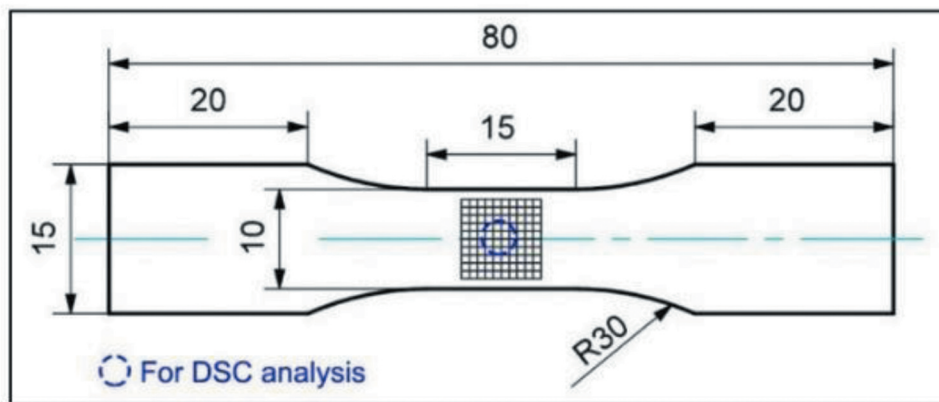


Figure 1. Dimensions of tensile samples (mm).

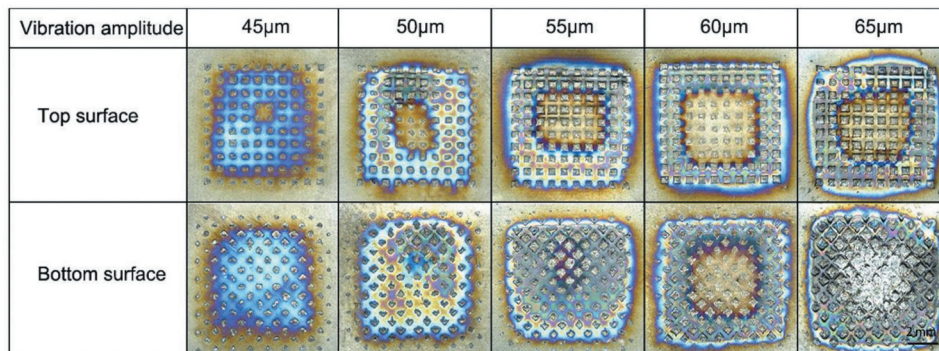


Figure 2. Surface appearances of the USWed NiTi joints obtained under different vibration amplitudes.

vibration amplitude increased, resulting in a temperature rise around the weld interface, which further leads to an increasing shear plastic deformation capacity on the weld surfaces. Consequently, the indentation depth on both surfaces became more significant, which could promote rapid formation of micro-welds and produce a superior joint.

The microstructural evolution at the welding interface of different joints was investigated by SEM, as presented in Fig. 3. For the 45  $\mu\text{m}$  joint, the interface near the weld center shows good bonding (black line shown in Fig. 3(a)), while unbonded regions can be observed at the weld edge near the top surface side (white dashed line shown in Fig. 3(b)). A similar welding interface appearance could be observed for the 50  $\mu\text{m}$  joint. However, the unbonded area at the periphery became smaller compared with the 45  $\mu\text{m}$  joint (depicted in Fig. 3(c,d)). When the vibration amplitude increased to 55  $\mu\text{m}$ , a completely well-bonded region was achieved along the whole weld region as shown in Fig. 3(e,f), which is beneficial to enhance the bonding strength of the NiTi joint. When the vibration amplitude further increased to 60 and 65  $\mu\text{m}$ , both good bonding area and fracture of Cu interlayer between the NiTi BM were observed as shown in Fig. 3(f,i) with black solid and dashed line boxes, respectively.

Another noteworthy phenomenon is that the Cu interlayer thickness in the well-bonded region along the weld interface varies significantly with increasing vibration amplitude: there is a decreasing tendency for the Cu layer thickness between the NiTi sheets, as evidenced in Fig. 3(a, c, e, g, i). At the weld interface center, the Cu foil experienced higher plastic deformation when compared to the NiTi BM due to its lower yield strength and thickness. The material flow and plastic deformation volume of the welded area increased with increasing vibration amplitude due to the increment of the frictional heat.<sup>[26,28,29]</sup> Therefore, when a significantly higher vibration amplitude (>60  $\mu\text{m}$ ) was applied, excessive frictional energy intensity promoted the formation of microcracks in the Cu interlayer (Fig. 3(h,j)).

To further clarify the deformation behavior of NiTi and Cu at the weld interface, EBSD was performed on the well-bonded interface region as depicted in Fig. 3(e) with a white line box. The crystal orientation maps of NiTi sheet and Cu foil along the welding interface are presented in Fig. 4, with the black lines corresponding to the grain boundaries. Compared to the NiTi side, there was a more substantial change in the microstructure of the Cu foil near the weld interface, which was composed of fine equiaxed grains (Fig. 4(b)). Meanwhile, several sub-grain boundaries were observed in the center of the Cu layer. Such can be related to the shear plastic deformation and subsequent recrystallization that occurred during the USW process. In particular, mechanical mixing was aided by the ultrasonic vibration sliding at the welding interface, which supported the Cu foil flow because of its lower yield strength aided by the frictional heat, contributing to the microstructural evolution and development of micro-bonds. Other works on USW also observed the formation of similar recrystallized microstructures.<sup>[30–32]</sup> It can be concluded that the Cu interlayer acts as a bonding bridge in the weld process through reaction and atomic migration, achieving joining between the NiTi sheets.

The phase transformation behaviors of the NiTi BM and welds obtained with multiple vibration amplitudes are depicted in Fig. 5, where B19' corresponds to martensite and B2 to austenite. The start (s) and finish (f) temperatures of austenite (A) and martensite (M) phase transformations were determined based on the ASTM-F2004-00 standard, and are summarized in Table 1. At room temperature, both the NiTi BM and USW specimens were fully austenitic. The onset temperatures for  $M_s$  and  $A_f$  of the joints ranged between  $-34 \pm 2^\circ\text{C}$  and  $-7 \pm 2^\circ\text{C}$ , respectively, with a hysteresis ranging from 26 to 30°C.

From the DSC measurements, it is noticeable that both the NiTi BM and welds exhibited a one-step phase transformation from B2 austenite to B19' martensite during the cooling process, without evidence of R-phase transformation, which had been reported in USWed NiTi joints without the addition of Cu interlayer.<sup>[16]</sup> Besides, both the forward and reverse transformation behaviors showed a minor shift to lower temperatures upon cooling and to higher temperatures upon heating after USW. The transformation temperatures of NiTi can be affected by several features, namely, existence of precipitates, dislocation density, average grain size, thermal stresses, and detwinning.<sup>[33]</sup> Increasing of the austenite transformation temperatures are also known to occur by minor alterations in the composition of the weld. In fact, preferential Ni depletion drastically increases the transformation temperatures of Ni-rich NiTi alloys.<sup>[34]</sup> Furthermore, residual stresses, which occur during USW as a result of the combined effect of heating and plastic deformation, may also effectively impact the transformation temperatures of the material.<sup>[35]</sup>

Figure 6 shows the tensile load–displacement curves of the NiTi joints of different vibration amplitudes. The maximum tensile load of the USW joints firstly increased with the vibration amplitude varying from 45 to 55  $\mu\text{m}$ . The 55  $\mu\text{m}$  joint exhibited the best tensile performance. The first yielding occurred for a tensile load of 515 N, which was the starting point of the stress-induced martensitic transformation. The stress plateau corresponded to the detwinning of martensite.<sup>[36]</sup> Following the constant stress plateau, there was an increase in the required load to promote deformation, where elastic and subsequent plastic deformation of the detwinned martensitic structure occurred,<sup>[37]</sup> with fracture occurring at a tensile load of 693 N. Further increasing of the vibration amplitude resulted in decreased ultimate tensile load.

During the USW process, increasing the vibration amplitude creates a competition between two counterbalancing behaviors.<sup>[38]</sup> One is the increasing interfacial bonding strength, which is responsible for improving the joint strength. While sheet thinning is also observed, which reduces the resistant cross-section and therefore decreases the maximum load supported by the joint. The combination of both effects determines the final mechanical response of the USW joints. For low vibration amplitudes, insufficient bonding translated into interfacial failure, while for high vibration amplitudes, the joint failed through the thinner NiTi near the border of the weld zone. The maximum tensile load was obtained at an intermediate vibration amplitude where a good balance of bonding strength and material thinning was achieved.

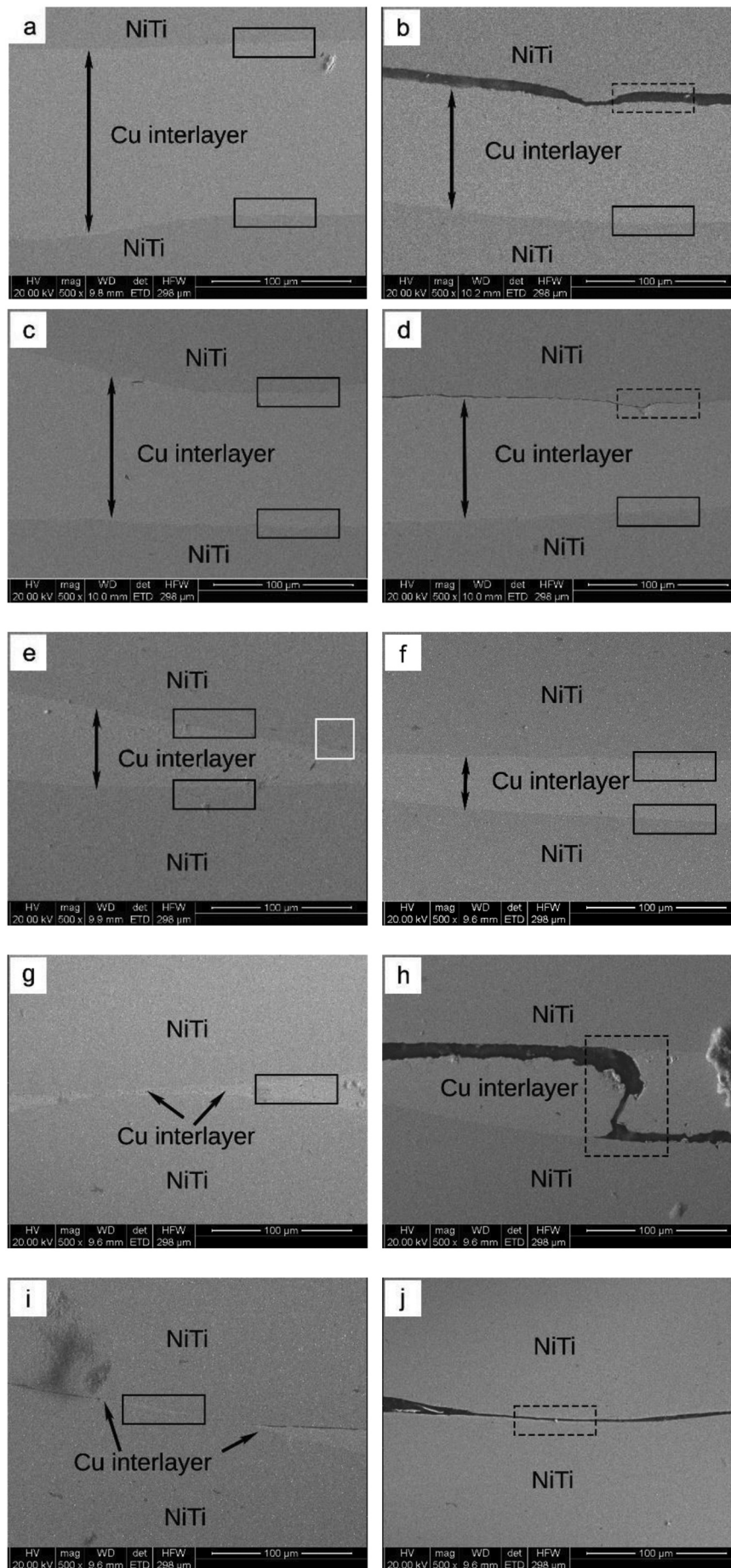


**Figure 3.** SEM imaging of joints obtained with different vibration amplitudes: (a) and (b) 45  $\mu\text{m}$  joint; (c) and (d) 50  $\mu\text{m}$  joint; (e) and (f) 55  $\mu\text{m}$  joint; (g) and (h) 60  $\mu\text{m}$  joint; (i) and (j) 65  $\mu\text{m}$  joint. (a), (c), (e), (g) and (i) all correspond to the center of the joints, whereas (b), (d), (f), (h) and (j) correspond to the periphery of the joints.

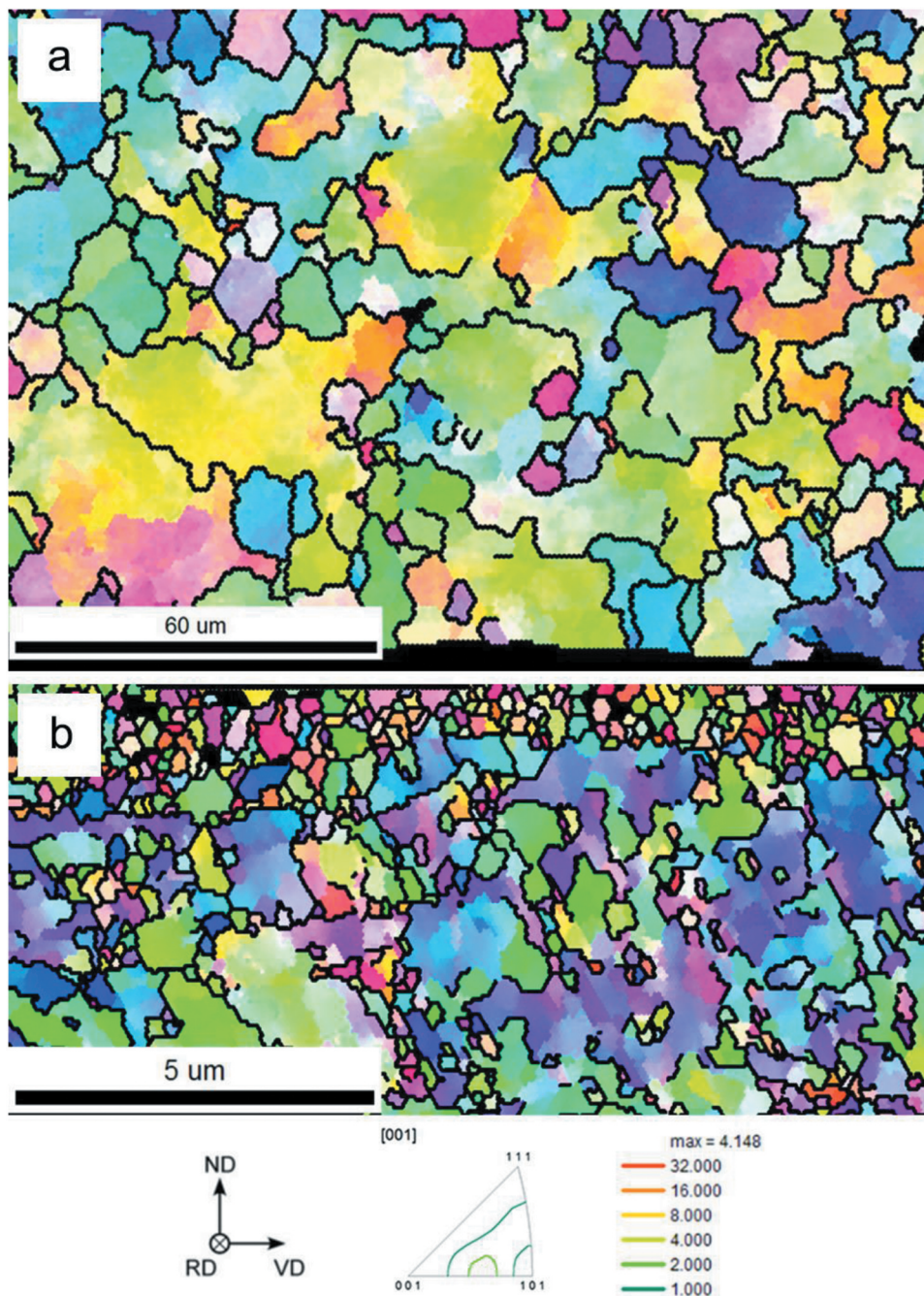


Figure 4. EBSD measurements performed on: (a) NiTi sheet; (b) Cu foil nearby joint interface.

Figure 7 depicts the images of the tensile fracture samples, where four different fracture modes are observed. The experimental observations indicated that the 45  $\mu\text{m}$  joint fractured along the weld interface, while the 50  $\mu\text{m}$  joint failed through the upper NiTi. The fracture mode changed to BM fracture away from the weld spot with necking occurred when a 55  $\mu\text{m}$  vibration amplitude was applied, after which fracture occurred at the edge of the weld spot, which was attributed to the reduced thickness of the welded region arising from the excessive heating generation at higher vibration amplitude.<sup>[26]</sup>

To clarify the influences of vibration amplitude on the quality of the obtained joints, the fracture morphologies are shown in Fig. 8 (the observation locations were depicted with white line boxes in Fig. 7). Figure 8(a) depicts the fracture morphology

of the 45  $\mu\text{m}$  joint. Both flat-looking surface of NiTi (Fig. 8(b)) and dimples of Cu (Fig. 8(c)) can be observed, which show the characteristics of brittle-like and ductile fracture, respectively. The existence of discontinuities throughout the joining interface (Fig. 3(b)) can act as stress concentrators, thus aiding fracture initiation at the interface and then propagating along the Cu interlayer. For the 50  $\mu\text{m}$  joint, the fracture surface shows a mixed morphology composed of dimples of NiTi (Fig. 8(e)) and slip planes of Cu foil (Fig. 8(f)), suggesting that the center of the weld interface has a higher bonding strength than that of the upper NiTi material with plastic indentation. Fracture analysis of the 55  $\mu\text{m}$  joint revealed a ductile failure as illustrated by the massive presence of dimples of the NiTi BM (Fig. 8(g)), suggesting that the tensile lap-shear strength of the joint was superior

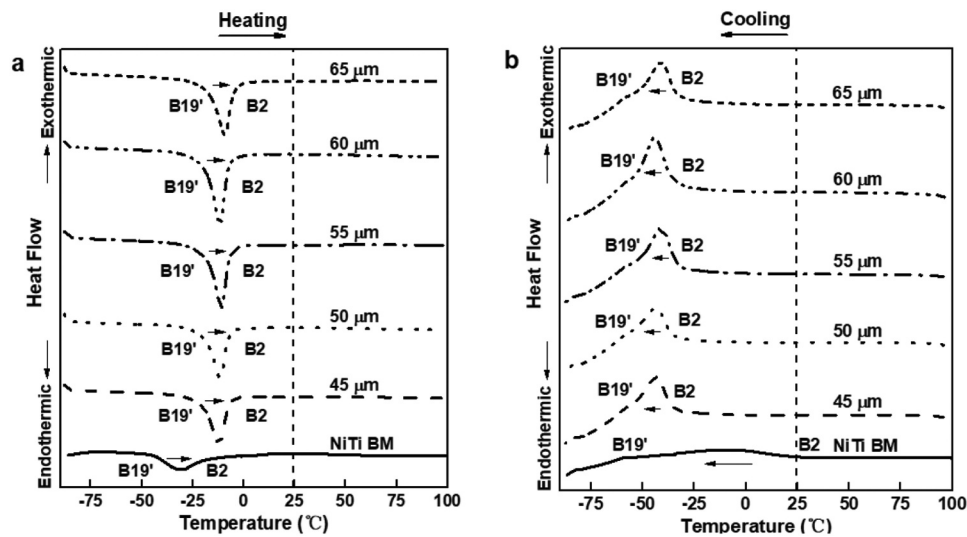


Figure 5. DSC results of the BM and welds: (a) heating, (b) cooling.

Table 1. Summary of the transformation temperatures ( $^{\circ}\text{C}$ ) of the NiTi BM and welds.

Reference	$A_s$	$A_f$	$M_s$	$M_f$
NiTi BM	-45.43	-27.87	22.91	-9.08
45 $\mu\text{m}$	-19.90	-6.77	-35.59	-57.29
50 $\mu\text{m}$	-19.10	-7.44	-35.43	-58.51
55 $\mu\text{m}$	-18.24	-6.38	-33.21	-52.13
60 $\mu\text{m}$	-18.74	-8.19	-35.34	-56.40
65 $\mu\text{m}$	-17.12	-6.14	-33.28	-55.78

than that of the BM. Figure 8(h,i) shows the case of a 60  $\mu\text{m}$  joint which failed along the border of the weld. When observing the fracture surface, it can be noticed that Cu was well bonded

with NiTi as shown in Fig. 8(i), while the NiTi was overthinned due to the severe plastic deformation when higher vibration amplitude applied as depicted by the black line in Fig. 8(h). Moreover, some notches can be noticed on the fracture surface of NiTi as the white arrows depicted in Fig. 8(i), suggesting that the crack initiated from these notches and then propagated along the NiTi sheet until the final fracture.

## Conclusions

NiTi SMAs were ultrasonic spot welded with a Cu interlayer under different varying vibration amplitudes. The microstructure

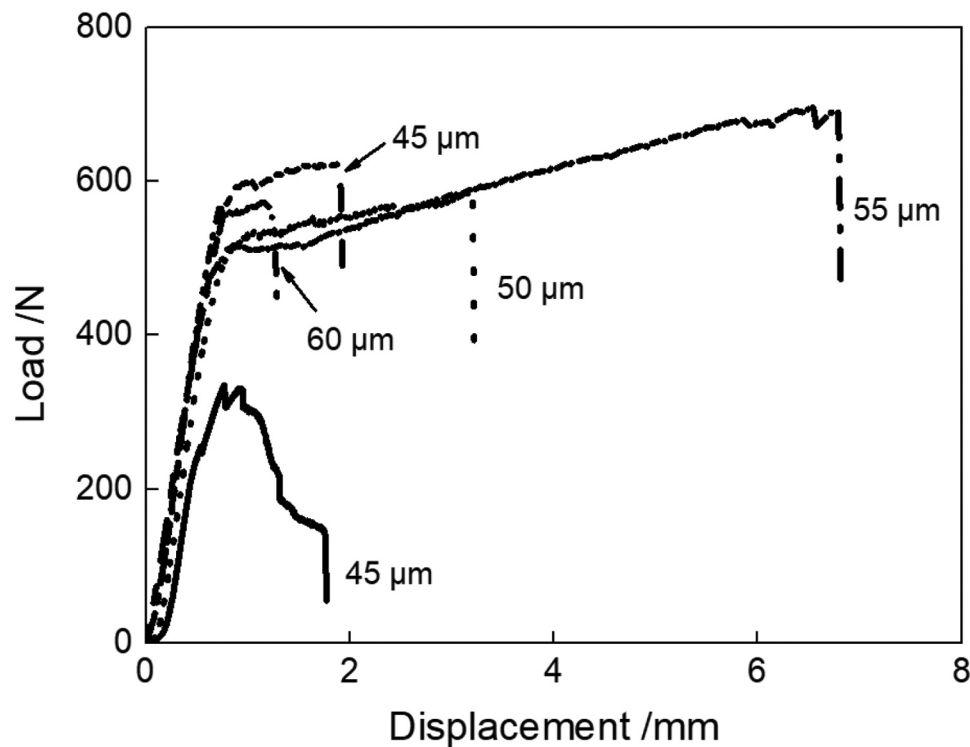


Figure 6. Tensile load-displacement curves of USWed NiTi joints for different vibration amplitudes.



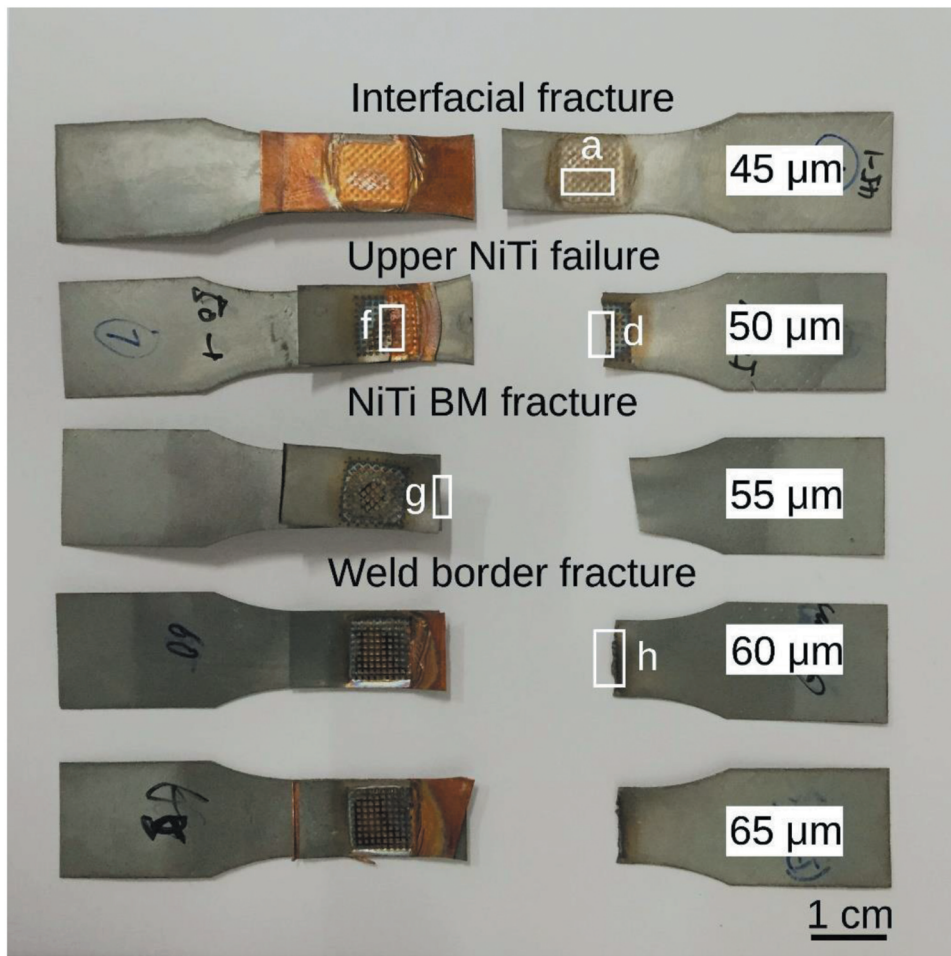


Figure 7. Effect of vibration amplitudes on fracture patterns developed in tensile lap-shear tests.

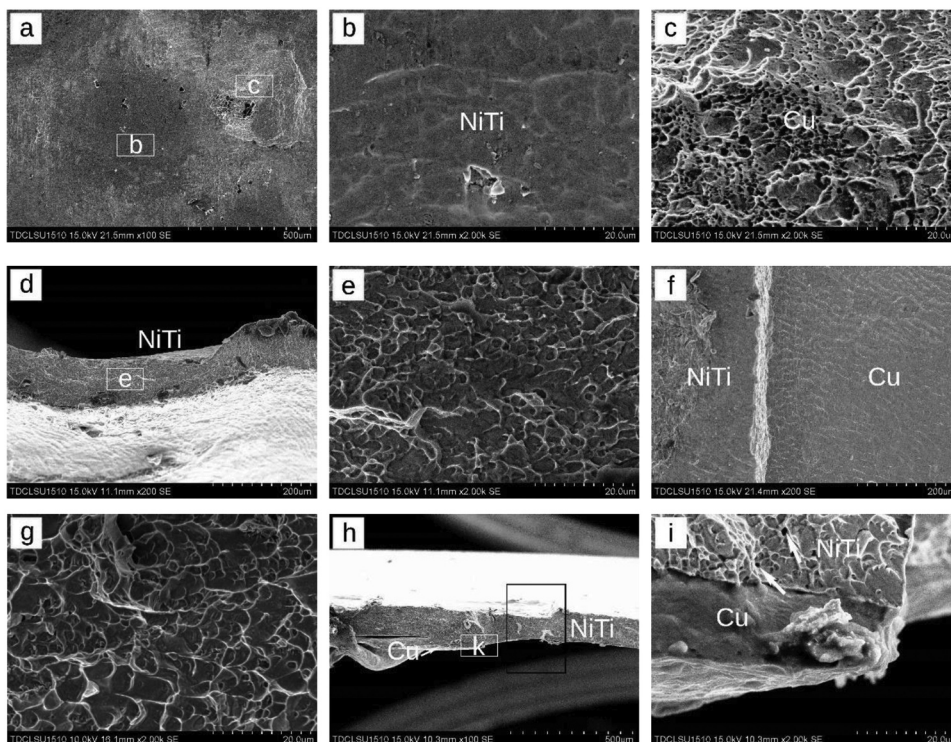


Figure 8. Fracture morphology of NiTi joints obtained with different vibration amplitudes: (a)-(c) 45 μm joint, (d)-(f) 50 μm joint, (g) 55 μm joint, (h) and (i) 60 μm joint.

and performances of the NiTi joints were analyzed in detail. The following main conclusions can be drawn:

- (1) When the vibration amplitude increased from 45 to 65  $\mu\text{m}$ , more severe plastic deformation of the NiTi BM and Cu foil was generated, leading to an increase of the indentation depth on the weld surface and reduction of the Cu foil thickness at the weld interface.
- (2) The optimized vibration amplitude contributed to the better bonding interface, and a recrystallized microstructure can be observed at the position of Cu foil.
- (3) The phase transformation temperatures of the NiTi joints were altered after welding, with decreasing martensite transformation temperature and increasing austenite transformation temperature occurring during cooling and heating, respectively.
- (4) During the tensile lap-shear tests, four different fracture modes were observed with varying vibration amplitudes. The maximum ultimate tensile load was achieved when a 55  $\mu\text{m}$  vibration amplitude was applied and a ductile fracture surface of the NiTi BM was observed.

## Acknowledgments

JPO acknowledges the Fundação para a Ciência e Tecnologia (FCT) for its support via the project UID/00667/2020 (UNIDEMI).

## Funding

This work was supported by The Chinese Civil Aviation Administration [No. U1933129], The Chinese National Key Program [No.2018YFB1107900], Natural Science Foundation of Tianjin City [No. 18JQJNJC04100, No.19JCZDJC39000, and 19YFFCYS00090].

## ORCID

W. Zhang  <http://orcid.org/0000-0001-6471-7412>

## References

- [1] Oliveira, J. P.; Miranda, R. M.; Braz Fernandes, F. M. Welding and Joining of NiTi Shape Memory Alloys: A Review. *Prog. Mater. Sci.* **2017**, *88*, 412–466. DOI: [10.1016/j.pmatsci.2017.04.008](https://doi.org/10.1016/j.pmatsci.2017.04.008).
- [2] Birnbaum, A. J.; Yao, Y. L. The Effects of Laser Forming on NiTi Superelastic Shape Memory Alloys. *ASME J. Manuf. Sci. Eng.* **2010**, *132*(4), 041002. DOI: [10.1115/1.4000309](https://doi.org/10.1115/1.4000309).
- [3] Melly, S. K.; Liu, L. W.; Liu, Y. J.; Leng, J. S. Active Composites Based on Shape Memory Polymers: Overview, Fabrication Methods, Applications, and Future Prospects. *J. Mater. Sci.* **2020**, *55*(25), 10975–11051. DOI: [10.1007/s10853-020-04761-w](https://doi.org/10.1007/s10853-020-04761-w).
- [4] Zeng, Z.; Cong, B. Q.; Oliveira, J. P.; Ke, W. C.; Schell, N.; Peng, B.; Qi, Z. W.; Ge, F. G.; Zhang, W.; Ao, S. S. Wire and Arc Additive Manufacturing of a Ni-rich NiTi Shape Memory Alloy: Microstructure and Mechanical Properties. *Addit. Manuf.* **2020**, *32*, 101051. DOI: [10.1016/j.addma.2020.101051](https://doi.org/10.1016/j.addma.2020.101051).
- [5] Andani, M. T.; Saedi, S.; Turabi, A. S.; Karamooz, M. R.; Haberland, C.; Karaca, H. E.; Elahinia, M. Mechanical and Shape Memory Properties of Porous Ni<sub>50</sub>Ti<sub>49.9</sub> Alloys Manufactured by Selective Laser Melting. *J. Mech. Behav. Biomed. Mater.* **2017**, *68*, 224–231. DOI: [10.1016/j.jmbbm.2017.01.047](https://doi.org/10.1016/j.jmbbm.2017.01.047).
- [6] Ao, S. S.; Li, K. B.; Liu, W. D.; Qin, X. Y.; Wang, T.; Dai, Y.; Luo, Z. Electrochemical Micromachining of NiTi Shape Memory Alloy with Ethylene glycol–NaCl Electrolyte Containing Ethanol.

- J. Manuf. Process.* **2020**, *53*, 223–228. DOI: [10.1016/j.jmapro.2020.02.019](https://doi.org/10.1016/j.jmapro.2020.02.019).
- [7] Zeng, Z.; Yang, M.; Oliveira, J. P.; Song, D.; Peng, B. Laser Welding of NiTi Shape Memory Alloy Wires and Tubes for Multi-functional Design Applications. *Smart Mater. Struct.* **2016**, *25*(8), 085001. DOI: [10.1088/0964-1726/25/8/085001](https://doi.org/10.1088/0964-1726/25/8/085001).
- [8] Tam, B.; Khan, M. I.; Zhou, Y. Mechanical and Functional Properties of Laser-welded Ti-55.8 Wt Pct Ni Nitinol Wires. *Metall. Mater. Trans. A.* **2011**, *42*(8), 2166–2175. DOI: [10.1007/s11661-011-0639-6](https://doi.org/10.1007/s11661-011-0639-6).
- [9] Shamsolhodaei, A.; Sun, Q.; Wang, X.; Panton, B.; Di, H.; Zhou, Y. N. Effect of Laser Positioning on the Microstructure and Properties of NiTi-copper Dissimilar Laser Welds. *J. Mater. Eng. Perform.* **2020**, *29*(2), 849–857. DOI: [10.1007/s11665-020-04637-9](https://doi.org/10.1007/s11665-020-04637-9).
- [10] Mehrpouya, M.; Gisario, A.; Barletta, M.; Natali, S.; Veniali, F. Dissimilar Laser Welding of NiTi Wires. *Lasers Manuf. Mater. Process.* **2019**, *6*, 99–112. DOI: [10.1007/s40516-019-00084-0](https://doi.org/10.1007/s40516-019-00084-0).
- [11] Watanabe, T.; Itoh, H.; Yanagisawa, A.; Hiraishi, M. Ultrasonic Welding of Heat Treatable Aluminum Alloy A6061 Sheet. *Weld. Int.* **2009**, *23*(9), 633–639. DOI: [10.1080/09507110902842802](https://doi.org/10.1080/09507110902842802).
- [12] Rubino, F.; Parmar, H.; Esperto, V.; Carlone, P. Ultrasonic Welding of Magnesium Alloys: A Review. *Mater. Manuf. Process.* **2020**, *35*(10), 1051–1068. DOI: [10.1080/10426914.2020.1758330](https://doi.org/10.1080/10426914.2020.1758330).
- [13] Li, M. F.; Zhu, Z. Q.; Xiao, Q. K.; Zhang, Y. F. Mechanical Properties and Microstructure Evolution of Dissimilar Mg and Al Alloys Welded Using Ultrasonic Spot Welding. *Mater. Res. Express.* **2019**, *6*(8), 086588. DOI: [10.1088/2053-1591/ab2010](https://doi.org/10.1088/2053-1591/ab2010).
- [14] Luo, Y.; Chung, H.; Cai, W.; Rinker, T.; Hu, S. J.; Kannatey-Asibu, E.; Abell, J. Joint Formation in Multilayered Ultrasonic Welding of Ni-coated Cu and the Effect of Preheating. *ASME J. Manuf. Sci. Eng.* **2018**, *140*(11), 111003. DOI: [10.1115/1.4040878](https://doi.org/10.1115/1.4040878).
- [15] Feng, M. N.; Chen, Y.; Fu, D. H.; Qu, C.; Luo, Z. Fatigue Behaviour and Life Estimation of Mg/Al Ultrasonic Spot Weld Bonding Welds. *Sci. Technol. Weld. Join.* **2018**, *23*(6), 487–500. DOI: [10.1080/13621718.2017.1417782](https://doi.org/10.1080/13621718.2017.1417782).
- [16] Zhang, W.; Ao, S. S.; Oliveira, J. P.; Zeng, Z.; Luo, Z.; Hao, Z. Z. Effect of Ultrasonic Spot Welding on the Mechanical Behaviour of NiTi Shape Memory Alloys. *Smart Mater. Struct.* **2018**, *27*(8), 085020. DOI: [10.1088/1361-665X/aacfeb](https://doi.org/10.1088/1361-665X/aacfeb).
- [17] Oliveira, J. P.; Panton, B.; Zeng, Z.; Andrei, C. M.; Zhou, Y.; Miranda, R. M.; Braz Fernandes, F.-M. Laser Joining of NiTi to Ti6Al4V Using a Niobium Interlayer. *Acta Mater.* **2016**, *105*, 9–15. DOI: [10.1016/j.actamat.2015.12.021](https://doi.org/10.1016/j.actamat.2015.12.021).
- [18] Zeng, Z.; Panton, B.; Oliveira, J. P.; Han, A.; Zhou, Y. N. Dissimilar Laser Welding of NiTi Shape Memory Alloy and Copper. *Smart Mater. Struct.* **2015**, *24*, 125036. DOI: [10.1088/0964-1726/24/12/125036](https://doi.org/10.1088/0964-1726/24/12/125036).
- [19] Bricknell, R. H.; Melton, K. N.; Mercier, O. The Structure of NiTiCu Shape Memory Alloys. *Metall. Trans. A.* **1979**, *10*, 693–697. DOI: [10.1007/BF02658390](https://doi.org/10.1007/BF02658390).
- [20] Gugel, H.; Schuermann, A.; Theisen, W. Laser Welding of NiTi Wires. *Mater. Sci. Eng. A.* **2008**, *481–482*, 668–671. DOI: [10.1016/j.msea.2006.11.179](https://doi.org/10.1016/j.msea.2006.11.179).
- [21] Li, H. M.; Sun, D. Q.; Gu, X. Y.; Dong, P.; Lv, Z. P. Effects of the Thickness of Cu Filler Metal on the Microstructure and Properties of Laser-welded TiNi Alloy and Stainless Steel Joint. *Mater. Des.* **2013**, *50*, 342–350. DOI: [10.1016/j.matdes.2013.03.014](https://doi.org/10.1016/j.matdes.2013.03.014).
- [22] Shojaei Zoeram, A.; Akbari Mousavi, S. A. A. Effect of Interlayer Thickness on Microstructure and Mechanical Properties of as Welded Ti6Al4V/Cu/NiTi Joints. *Mater. Lett.* **2014**, *133*, 5–8. DOI: [10.1016/j.matlet.2014.06.141](https://doi.org/10.1016/j.matlet.2014.06.141).
- [23] Zhang, W.; Ao, S. S.; Oliveira, J. P.; Zeng, Z.; Huang, Y. F.; Luo, Z. Microstructural Characterization and Mechanical Behavior of NiTi Shape Memory Alloys Ultrasonic Joints Using Cu Interlayer. *Materials.* **2018**, *11*(10), 1830. DOI: [10.3390/ma11101830](https://doi.org/10.3390/ma11101830).
- [24] Zhang, W.; Ao, S. S.; Oliveira, J. P.; Li, C. J.; Zeng, Z.; Wang, A. Q.; Luo, Z. On the Metallurgical Joining Mechanism during Ultrasonic Spot Welding of NiTi Using a Cu Interlayer. *Scr. Mater.* **2020**, *178*, 414–417. DOI: [10.1016/j.scriptamat.2019.12.012](https://doi.org/10.1016/j.scriptamat.2019.12.012).

- [25] Hall, E. O. Variation of Hardness of Metals with Grain Size. *Nature*. 1954, 173(4411), 948–949. DOI: [10.1038/173948b0](https://doi.org/10.1038/173948b0).
- [26] Das, S.; Satpathy, M. P.; Pattanaik, A.; Routara, B. C. Experimental Investigation on Ultrasonic Spot Welding of Aluminum-cupronickel Sheets under Different Parametric Conditions. *Mater. Manuf. Process.* 2019, 34(15), 1689–1700. DOI: [10.1080/10426914.2019.1689265](https://doi.org/10.1080/10426914.2019.1689265).
- [27] Ni, Z. L.; Ye, F. X. Effect of Lap Configuration on the Microstructure and Mechanical Properties of Dissimilar Ultrasonic Metal Welded Copper-aluminum Joints. *J. Mater. Process. Technol.* 2017, 245, 180–192. DOI: [10.1016/j.jmatprotec.2017.02.027](https://doi.org/10.1016/j.jmatprotec.2017.02.027).
- [28] De Leon, M.; Shin, H. S. Weldability Assessment of Mg Alloy (AZ31B) Sheets by an Ultrasonic Spot Welding Method. *J. Mater. Process. Technol.* 2017, 243, 1–8. DOI: [10.1016/j.jmatprotec.2016.11.022](https://doi.org/10.1016/j.jmatprotec.2016.11.022).
- [29] Satpathy, M. P.; Mohapatra, K. D.; Sahoo, S. K.; Ultrasonic Spot Welding of Al–Cu Dissimilar Metals: A Study on Parametric Influence and Thermo-mechanical Simulation. *Int. J. Model. Simul.* 2018, 38(2), 83–95. DOI: [10.1080/02286203.2017.1395198](https://doi.org/10.1080/02286203.2017.1395198).
- [30] Fujii, H. T.; Goto, Y.; Sato, Y. S.; Kokawa, H. Microstructure and Lap Shear Strength of the Weld Interface in the Ultrasonic Welding of Al Alloy to Stainless Steel. *Scr. Mater.* 2016, 116, 135–138. DOI: [10.1016/j.scriptamat.2016.02.004](https://doi.org/10.1016/j.scriptamat.2016.02.004).
- [31] Fujii, H. T.; Sriraman, M. R.; Babu, S. S. Quantitative Evaluation of Bulk and Interface Microstructure in Al-3003 Alloy Builds Made by Very High Power Ultrasonic Additive Manufacturing. *Metall. Mater. Trans. A*. 2011, 42(13), 4045–4055. DOI: [10.1007/s11661-011-0805-x](https://doi.org/10.1007/s11661-011-0805-x).
- [32] Fujii, H. T.; Endo, H.; Sato, Y. S.; Kokawa, H. Interfacial Microstructure Evolution and Weld Formation during Ultrasonic Welding of Al Alloy to Cu. *Mater. Charact.* 2018, 139, 233–240. DOI: [10.1016/j.matchar.2018.03.010](https://doi.org/10.1016/j.matchar.2018.03.010).
- [33] Mani Prabu, S. S.; Madhu, H. C.; Perugu, C.-S.; Akash, K.; Ajay Kumar, P.; Kailas, S. V.; Anbarasu, M.; Palani, I. A. Microstructure, Mechanical Properties and Shape Memory Behaviour of Friction Stir Welded Nitinol. *Mater. Sci. Eng. A*. 2017, 693, 233–236. DOI: [10.1016/j.msea.2017.03.101](https://doi.org/10.1016/j.msea.2017.03.101).
- [34] Otsuka, K.; Ren, X. Physical Metallurgy of Ti-Ni-based Shape Memory Alloys. *Prog. Mater. Sci.* 2005, 50, 511–678. DOI: [10.1016/j.pmatsci.2004.10.001](https://doi.org/10.1016/j.pmatsci.2004.10.001).
- [35] Liu, Y.; Galvin, S. P. Criteria for Pseudoelasticity in Near-equiatomic NiTi Shape Memory Alloys. *Acta Mater.* 1997, 45, 4431–4439. DOI: [10.1016/S1359-6454\(97\)00144-4](https://doi.org/10.1016/S1359-6454(97)00144-4).
- [36] Li, Q.; Zhu, Y. X.; Guo, J. L. Microstructure and Mechanical Properties of Resistance-welded NiTi Stainless Steel Joints. *J. Mater. Process. Technol.* 2017, 249, 538–548. DOI: [10.1016/j.jmatprotec.2017.07.001](https://doi.org/10.1016/j.jmatprotec.2017.07.001).
- [37] Ijaz, M. F.; Heraud, L.; Castany, P.; Thibon, I.; Gloriant, T. Superelastic Behavior of Biomedical Metallic Alloys. *Metall. Mater. Trans. A*. 2020, 51, 3733–3741. DOI: [10.1007/s11661-020-05840-y](https://doi.org/10.1007/s11661-020-05840-y).
- [38] Ni, Z. L.; Ye, F. X. Dissimilar Joining of Aluminum to Copper Using Ultrasonic Welding. *Mater. Manuf. Process.* 2016, 31(16), 2091–2100. DOI: [10.1080/10426914.2016.1221101](https://doi.org/10.1080/10426914.2016.1221101).